Electro-thermal micro-pumps: exploiting structural polarizations at smeared interfaces

M. Stubbe* and J. Gimsa*

*University of Rostock, Gertrudenstr. 11A, 18057 Rostock, Germany, jan.gimsa@uni-rostock.de

ABSTRACT

Various designs for new AC electro-thermal micro-pumps (ETµPs) have been presented which exploit AC electro-kinetic forces acting on smeared charges in the bulk of fluids in the presence of a temperature gradient. In some designs, an integrated heating element allows the temperature gradient to be adjusted. The advantages of the ETµP principle are the absence of moving parts, the opportunity to passivate all the pump structures, homogeneous pump channel cross sections reducing the risk of the channel clogging due to debris, force plateaux in broad frequency ranges, as well as a reversal of the pump direction, depending on the driving frequency (kHz to GHz). The integration of additional inductances permits an increase of the pump velocity at low AC field voltages at resonance conditions. This and the usable conductivity range of the pumping medium from extremely low to above physiological values predestine ETµPs for integration in biological analysis systems such as lab-on-chip systems.

Keywords: induced dipole moment, lab-on-chip systems, ponderomotive volume force, RC model, structural dispersion

1 INTRODUCTION

In many micro-total analysis systems (µ-TAS) and lab-on-chip systems (LOCs) micro-fluidic structures and pumps are integrated for the manipulation of small volumes of fluids [1,2]. These pumps are based on a variety of principles, e.g. travelling wave dielectrophoresis (TWD) [3-6], or DC and AC electro-osmosis (EO) [7,8]. Pumps using inhomogeneous AC electric fields usually work with small inter-electrode gaps of around 25 µm and up to 100 µm [7-9]. This is especially so when the pumps are based on AC electro-osmosis (EO) at frequencies below 1 MHz, small inter-electrode gaps (5-100 µm) and high electrode voltages have been shown to increase efficiency [7-9]. High electrode voltages in combination with small inter-electrode gaps result in high electric field strengths, which may damage the integrity of biological membranes and induce membrane pores by dielectric breakdown [10-13].

Naturally enough, lower electrode voltages, as well as the lower field strengths obtained with larger electrode gaps, electrode passivation and smaller electrode curvatures reduce the probability of membrane breakdown and the risk of cell damage. Moreover, the lower local current densities and the reduced electrolytic processes will increase the lifetime of the pump structures.

The pump principles of the ETµPs are based on the interaction of an AC field with smeared polarization charges induced in the bulk of fluid media. In homogeneous media, these charges are induced by the external field in the presence of electric property gradients, caused by temperature gradients. While the conductivity of aqueous media increases ($2.3\%K^{-1}$), its permittivity decreases ($0.4\%K^{-1}$). The temperature gradients can be generated by external or integrated heating elements, electromagnetic radiation or Joule heating by the pump field itself [5,16-19]. In the presence of an external field, the continuous change of the electric properties along the temperature gradient results in a smeared medium polarization while the interaction of the external field with ion and dipole charges induce an electro-quasistatic volume force. The effect can be considered a spatially smeared Maxwell–Wagner bulk polarization. Accordingly, the forces induced in the polarized fluid volume with smeared borders depend on the frequency of the AC electric field [20]. Negative or positive forces may be induced, depending on whether the pump effect is based on the conductivity or permittivity polarization of the medium [19,20]. The transition from a domination of the conductivity to the permittivity polarization is observed at the (characteristic) Maxwell-Wagner frequency.

In ETµPs, the pump force generation is based on the in-phase component of the induced smeared medium polarization [16-19]. ETµPs exhibit broad force plateaus with transitions at characteristic dispersion frequencies. Another advantage of ETµPs is the inhibition of backflow because the pump force is generated throughout the entire volume of the pump medium between the field electrodes. This force is based on a temperature gradient in the range of a largely homogeneous AC electric field [16-19], a temperature peak in the range of an AC field gradient or a combination of the two gradients [18].

Typically, ETµPs consist of a homogeneous channel structure with a heating element and field electrodes [14-19]. Large field-electrode gaps of 390 µm and more were used. The pump velocity was controlled by the temperature gradient resulting from the balance of Joule medium heating by the AC pump field and the heating element which introduced an asymmetric temperature distribution with respect to the field electrodes [14-19]. Additionally, the use of AC driving fields allowed for the passivation of all electric pump structures, e.g. by SiO_2 or Si_3N_4 [14,15].

2 MATERIAL AND METHODS

2.1 Pump structure and measuring setup

Different ETµP chip designs were processed on glass carriers by micro-systems technology (Fig. 1). The AC-field electrodes and an optional DC-heating element were photolithographically processed from a platinum layer (thickness 100 nm) on a 4" D263T thin-glass wafer (thickness 550 µm, Schott AG, Mainz, Germany). The manufacturing error of the photolithographic process was ±6 µm. The final ETµP chips had a size of 22×27 mm^2 and were compatible with standardized micro fluidic systems. Optionally, a SiO_2-passivation layer (thickness 630 nm) was introduced. The pump and fluid channel walls were integrated in a 60 µm thick photoresist structure, which was covered by a poly-dimethylsiloxane (PDMS) lid with inlets and outlets [16,17].

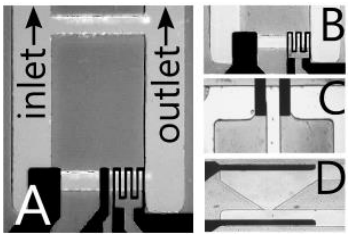

Fig. 1: Microscopic images of different ETµP designs (dark: platinum structures; light gray: polymer-wall structures; light areas: fluid channels). A and B are indirectly (separate ground-field electrode) and directly heated ETµPs with meander-heating elements, respectively. C and D have only field electrodes. A symmetry break is introduced by a T- (C) or a funnel-shaped pump channel (D). The square pump channel, as well as the channels to the external inlet and outlet filling nozzles are shown in A.

Measurements were conducted under an inverse microscope (Axiovert 100, Carl Zeiss AG, Oberkochen, Germany). The microscope camera was connected to a PC and the velocity was measured with a stopwatch and grids of different scaling. The pump medium could be exchanged by means of an external syringe pump (Diluter 4x, GeSiM GmbH, Grosserkmannsdorf, Germany) through filling nozzles with tube connectors in the PDMS lid. The DC heating and the sinusoidal field-electrode voltages were applied by a DC power supply (Voltcraft DPS-4005 PFC, Conrad Electronic SE, Hirschau, Germany) and a function generator (HP8116A Agilent Technologies, Santa Clara, CA, USA). An additional power amplifier (ENI 350L, ENI, Rochester, NY, USA) was used for higher driving voltages. The AC pump field voltage was controlled by an oscilloscope (HP54616C, Agilent Technologies, Santa Clara, CA, USA).

2.2 Pump media

Different pump medium conductivities (σ_M = 0.01, 0.1, and 1.0 Sm^{-1}) were adjusted with sodium chloride in distilled water. Pumping of cell-culture media with approximate conductivities of 1.2 Sm^{-1} was successfully tested. For velocity measurements, latex particles (Standard Dow Latex, Serva Electrophoresis GmbH, Heidelberg, Germany) of 835 nm diameter were used as flow markers. The latex particles could be traced under the microscope. The small size of the particles did not affect the pump flow and their sedimentation was very slow [16-18].

3 THEORY

The ETµP principle is based on the induction of electroquasistatic forces in the volume of dielectric fluids by the interaction of an AC electric field with separated ion or dipole charges. A temperature gradient in the medium is the prerequisite for influencing space charges. Fig. 2 shows the calculated temperature and electric field along the central axis of the pump channel of the ETµP shown in Fig. 1B, as well as the temperature difference ΔT between the field electrodes essential for the volume force generation. The electric field strength and the temperature distribution were calculated using the Finite Element Methode (FEM).

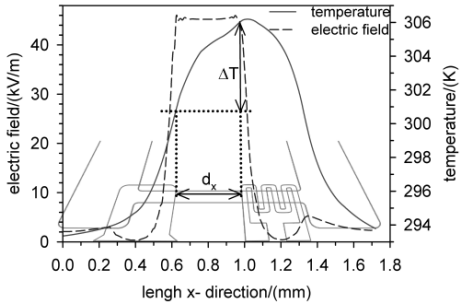

Fig. 2: FEM simulation of the temperature and AC-field disribution of the ETµP shown in Fig. 1B. The heating power, electrode voltage and medium conductivity were 13 mW (2.1 V_{DC} heating voltage), 20 V_{rms} and σ_M = 1.0 Sm^{-1}.

The time-averaged electric volume force $\langle F_e \rangle$ induced in the medium volume by the interaction of temperature-influenced space charges and the AC electric field can be described by

$$\left\langle \overrightarrow{F_e} \right\rangle = -\frac{1}{2}\left[\left(\frac{\nabla\sigma}{\sigma} - \frac{\nabla\varepsilon}{\varepsilon} \right) \cdot \vec{E}_0 \frac{\varepsilon \vec{E}_0}{1+(\omega\tau)^2} + \frac{1}{2}\left|E_0\right|^2 \nabla\varepsilon \right] \qquad (1)$$

with E and ω being the electric field strength and the angular frequency of the medium. The relaxation time $\tau = \varepsilon\sigma^{-1}$ depends on the permittivity and conductivity of the medium. After introducing a geometry coeffifient ϕ for the pump channel, the viscosity of the medium η and some mathematical simplifications, the pump force velocity can be estimated for the limiting cases of $\omega \to 0$ and $\omega \to \infty$ by Eqs. 2 and 3.

$$\lim_{\omega\to 0} v = -\frac{1}{2}\varepsilon \left|\overrightarrow{E_0}\right|^2 \Delta T \frac{\phi}{\eta}\left(0.022\, K^{-1}\right) \qquad (2)$$

$$\lim_{\omega\to \infty} v = -\frac{1}{2}\varepsilon \left|\overrightarrow{E_0}\right|^2 \Delta T \frac{\phi}{\eta}\left(-0.002\, K^{-1}\right) \qquad (3)$$

Furthermore, as has long been known, polarization phenomena can be described by equivalent circuit diagrams, e.g. resistor- capacitor (RC) models [21,22]. For a given geometry, our impedance analysis of the ETµP properties provided resistance and capacitance values, as well as for the external wiring.

The electric dispersion of aqueous media mediates the frequency-dependent transition from a domination of the medium current by the ion concentration-dependent conductivity to a domination of the permittivity, i.e. the displacement currents. The two current contributions are balanced at the characteristic Maxwell-Wagner frequency [21]. From the dispersion relation it follows that each volume element of an aqueous medium, such as the pump medium can be described by a parallel circuit of a resistor and a capacitor (RC model) [21,22].

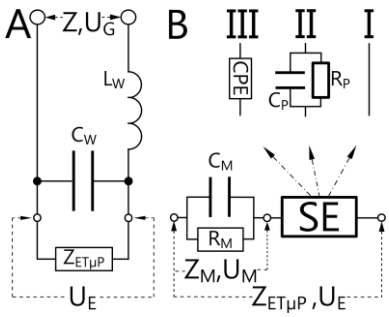

Fig. 3 Equivalent circuit diagrams of the external (A) and internal (B) ETµP elements. (A) and (B) present the external wiring of the ETµP and the impedance of the ETµP ($Z_{ETµP}$), respectively, with three different versions for the surface element (SE). Schemes I, II, and III stand for a fully bridged SE, the RC properties of a passivation layer, and a constant phase element (CPE), respectively. Indices W, P and M mark external wires, the passivation layer, and medium elements. U_G, U_E and U_M are the applied generator voltage, the field electrode voltage and the voltage drop over the pump medium. L_W represents the inductance of the wiring. Please note that the properties of the resistive heating element were not considered.

Electric, chemical, electrolytic and diffusion processes at the surfaces of the electrodes and within the electric double layers restrict the transition of current from the electronic conduction in the electrode metal into the ionic conduction in the aqueous solution at low frequencies. They may result in overpotentials. Electrically, these processes can be summarized by a CPE. In order to model the electrode-interface properties, we introduced an SE, which can either be described by the impedances of a CPE, a simple wire or an RC element, depending on the field frequency and a possible electrode passivation (Fig.1).

The RCL (resistor-capacitor-inductance) model of the full ETµP setup further includes the inductance and capacitance of the connecting external wiring. Coils that increase the wiring inductance can be used to generate a resonance peak in the pump field and to increase the pump velocity at low external driving voltages.

To sum up, the complete RCL model shown in Fig. 3 allowed us to describe the frequency-dependent pump velocity by means of the electrical properties of the aquaeous media, the temperature difference between the field electrodes, the electric properties of the passivation layer, the electric double layer properties, and the inductance of the external wiring.

4 RESULTS AND DISCUSSION

As predicted from Eqs. 2 and 3 and shown in Fig. 4, the pump velocity exhibits two plateaux in the lower and higher frequency ranges if no inductances influence the pump velocity.

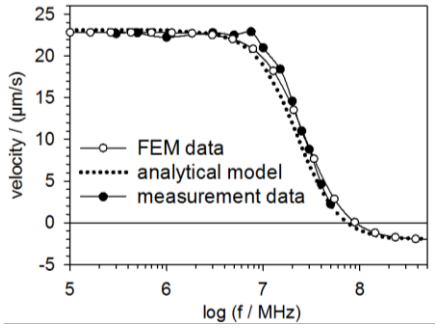

Fig. 4: Comparison of the pumping velocities of the measurement data, the FEM simulation, and the analytical model for the ETµP shown in Fig. 1A. The conductivity and relative permittivity of the pumping medium were 0.1 Sm^{-1} and 80 at a temperature of 293 K. The heating power and the pump field strength were 8 mW (2 V_{DC} heating voltage) and 31 kVm^{-1} (12 V_{rms} generator voltage between the field electrodes) resulting in a temperature difference across the field electrode distance of 8 K. The pump channel cross section area was 120×60 $µm^2$.

For ω→0, the volume force, and finally the pump velocity, is proportional to the sum of Coulomb and dielectric forces. At low frequencies, the conductive (Coulomb) force, i.e. the force related to conductivity effects, outweighs the overall pump force (Eq. (2)). For ω→∞ the frequency independent ionic conductivity is superseded by displacement currents, resulting in a domination of the dielectric force (Eq. (3)). The conductive and dielectric forces are oppositely oriented.

Fig. 4 also shows a large correspondence of the FEM, the extended analytical ETµP model and the measured pump velocities. The properties of the external wiring have been neglected in the FEM simulations.

Frequency-dependent pump velocity measurements, including additional inductances of 10 µH and 1 mH are shown in Fig. 5 for medium conductivities of 10 mSm^{-1}, 0.1 Sm^{-1} and 1 Sm^{-1}. A reversal of the pump flow could be observed for a conductivity of 10 mSm^{-1}, and an inductance of 10 µH (Fig. 5A). A strong increase in the pump velocity can be observed at the resonance frequency. This effect can be used to reach high pump velocities at low generator voltages.

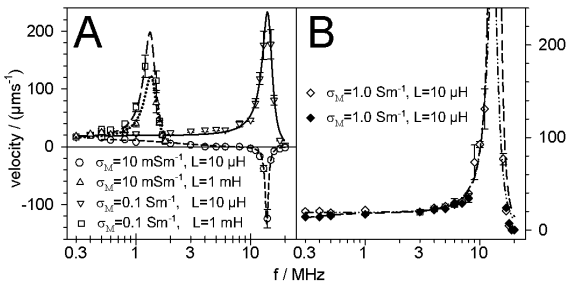

Fig. 5 Frequency-dependent pump velocities and fits of the equivalent diagram shown in Fig. 2 of non-passivated (outline symbols) and passivated (solid symbols) ETµPs with additional inductances of L=10 µH and 1 mH at medium conductivities σ_M of 10 mSm^{-1}, 0.1 Sm^{-1} and 1.0 Sm^{-1}. The heating and field electrode voltages were U_H=2.14 V_{DC} and U_G=20 V_{rms}.

In the case of passivated ETµPs, the pump velocity shows an increase in the lower frequency range (<20MHz), caused by the capacitive bridging of the SiO_2-passivation layer above the platinum field electrodes (compare to Fig. 4A) [16,18]. This effect can be used for a application-specific manipulation of the pump velocity in the lower frequency range. The passivation also protects the electrodes of electrolytic processes in this frequency range.

5 CONCLUSION

Various designs of the new AC electro-thermal micro-pumps exploit AC electro-kinetic forces acting in the volume of a fluid in the presence of a temperature gradient. The temperature gradient is induced by local Joule heating or separate heating elements. The temperature gradient creates conductivity and permittivity gradients in the polarizable pump medium in the prensence of which an external AC electric field influences smeared spatial charges. If there is also a symmetry break, the field-charge interaction results in an effective volumetric force leading to medium pumping, which can only be observed if the heating gradients and an AC pump field have been applied simultaneously. Measurements of the velocity of the pump flow dependence on the frequency and AC-field strength were consistent with medium velocities resulting from FEM simulations and an equivalent-circuit diagram. The advantages of the ETµP principle are the absence of moving parts, the opportunity to passivate all the pump structures, homogeneous pump channel cross sections reducing the risk of the channel clogging by debris, force plateaus in broad frequency ranges, as well as a reversal of the pump direction dependent on the driving frequency. The operating frequencies ranging from kHz to GHz prevent electrolytic processes and electrode deterioration. In some designs, an integrated heating element permits the temperature gradient to be adjusted. The integration of additional inductances allows for an increase of the pump velocity at low AC field voltages at resonance conditions. This and the usable conductivity range of the pumping medium from extremely low to above physiological values predestine ETµPs for integration in biological analysis. A further miniaturization of the pumps is also viewed as quite feasible. An increase in pump pressure and pump flow velocity can easily be achieved by placing multiple ETµPs in parallel or in series to an ETµP array.

REFERENCES

[1] T. Bourouina, A. Bossebuf and J.-P. Grandchamp, J. Micromech. Microeng., 7, 186–188, 1997.
[2] H. Andersson and A. van den Berg, Sens. Actuators B, 92, 315–325, 2003.
[3] J.R. Melcher and G.I. Taylor, Annu. rev. fluid mech., 1, 111–146, 1969.
[4] R.M. Ehrlich and J.R. Melcher, Phys. Fluids., 25, 1785-1793, 1982.
[5] M. Felten, P. Geggier, M. Jäger and C. Duschl, Phys. Fluids., 18, 51707(1-4), 2006.
[6] G. Fuhr, R. Hagedorn, T. Müller, W. Benecke, B. Wagner and J. Gimsa, Stud. biophys., 2, 79–102, 1991.
[7] V. Pretorius, B. Hopkins and J. Schieke, Journal of Chromatography A, 99, 23–30, 1974.
[8] A. Ajdari, Phys. Rev. E., 61, R45, 2000.
[9] A. Ramos, H. Morgan, N.G. Green and A. Castellanos, J. Phys. D: Appl. Phys., 31, 2338–2353, 1998.
[10] J.Gimsa, P. Marszalek, U. Loewe and T.Y. Tsong, Bioelectrochem. Bioenerg., 29, 81–89, 1992.
[11] E. Neumann and K. Rosenheck, J. Membr. Biol., 10, 279–290, 1972.
[12] U. Zimmermann, G. Pilwat and F. Riemann, Biophys. J., 14, 881–899, 1974.
[13] J. Gimsa and D. Wachner, Eur. Biophys. J., 30, 463–466, 2001.
[14] J. Gimsa and M. Holtappels, international Pat., WO/2005/001286, 2005.
[15] J. Gimsa, M. Holtappels and M. Stubbe, international Pat., WO/2007/098910, 2007.
[16] M. Stubbe, M. Holtappels and J. Gimsa, J. Phys. D: Appl. Phys., 40, 6850–6856, 2007.
[17] M. Holtappels, M. Stubbe and J. Gimsa, Phys. Rev. E, 79, 026309(1-10), 2009.
[18] M. Stubbe and J. Gimsa, Colloids Surf. A, 376, 97–101, 2011.
[19] M. Stubbe, A. Gyurova and J. Gimsa, Electrophoresis, 34, 562-574, 2012.
[20] J. Gimsa and M. Stubbe, Micro & Nano Fluidics Symposium, 2013, in this volume.
[21] K.W. Wagner, Arch. Elektrotech., 2, 371–387, 1914.
[22] K.R. Foster, H.P. Schwan, in: C. Polk, E. Postow, (Eds.): Handbook of biological effects of electromagnetic fields, 2nd ed., CRC Press, Boca Raton, 25–102, 1996

ACKNOWLEDGEMENTS

The authors thank Dr. W. Baumann for fruitful discussions and R. Sleigh for his help with the language.